# The phenol steam reforming reaction towards $H_2$ production on natural calcite

Domna A. Constantinou [a], José Luis G. Fierro [b], Angelos M. Efstathiou [a,*]

[a] Heterogeneous Catalysis Laboratory, Department of Chemistry, University of Cyprus, P.O. Box 20537, CY 1678 Nicosia, Cyprus
[b] Instituto de Catálisis y Petroleoquimica, CSIS, C/Marie Curie 2, Cantoblanco, 28049 Madrid, Spain

ABSTRACT

The steam reforming of phenol towards $H_2$ production was studied in the 650–800 °C range over a natural pre-calcined (air, 850 °C) calcite material. The effects of reaction temperature, water, hydrogen, and carbon dioxide feed concentrations, and gas hourly space velocity (GHSV, $h^{-1}$) were investigated. The increase of reaction temperature in the 650–800 °C range and water feed concentration in the 40–50 vol% range were found to be beneficial for catalyst activity and $H_2$-yield. A similar result was also obtained in the case of decreasing the GHSV from 85,000 to 30,000 $h^{-1}$. The effect of concentration of carbon dioxide and hydrogen in the phenol/water feed stream was found to significantly decrease the rate of phenol steam reforming reaction. The latter was probed to be related to the reduction in the rate of water dissociation as evidenced by the significant decrease in the concentration of adsorbed bicarbonate and –OH species on the surface of CaO according to in situ diffuse reflectance infrared Fourier transform spectroscopy (DRIFTS)-$CO_2$ adsorption experiments in the presence of water and hydrogen in the feed stream. Details of the $CO_2$ adsorption on the CaO surface at different reaction temperatures and gas atmospheres using in situ DRIFTS and transient isothermal adsorption experiments with mass spectrometry were obtained. Bridged, bicarbonate and unidentate carbonate species were formed under $CO_2/H_2O/He$ gas mixtures at 600 °C with the latter being the most populated. A substantial decrease in the surface concentration of bicarbonate and –OH species was observed when the CaO surface was exposed to $CO_2/H_2O/H_2/He$ gas mixtures at 600 °C, result that probes for the inhibiting effect of $H_2$ on the phenol steam reforming activity. Phenol steam reforming reaction followed by isothermal oxygen titration allowed the measurement of accumulated "carbonaceous" species formed during phenol steam reforming as a function of reaction temperature and short time on stream. An increase in the amount of "carbonaceous" species with reaction time (650–800 °C range) was evidenced, in particular at 800 °C (4.7 vs. 6.7 mg C/g solid after 5 and 20 min on stream, respectively).

© 2009 Elsevier B.V. All rights reserved.

## 1. Introduction

The increasing dependence on fossil fuels as energy source has caused serious environmental problems related to air pollution, acid rain, and climate changes leading to the urgent utilization of renewable energy sources as an alternative [1–4]. Biomass is abundantly available and is considered the only carbon source among all the other renewable energy sources that has a strong potential to be the starting material for the production of liquid fuels, chemicals, and hydrogen [5–7]. Hydrogen has been identified as an ideal energy carrier to support sustainable energy development and is receiving considerable attention for fuel cell applications [8,9].

The catalytic steam gasification of biomass appears to be an attractive technology for the production of hydrogen-rich gas and subsequent reduction of $CO_2$ emissions and other greenhouse gases [3,10–12]. However, the presence of tar in the produced gas is a significant impediment to the use of biomass in gasification systems for the production of clean gas for its further processing [3,4,7,10,12,13]. Condensation and polymerization of tar can cause clog of fuel lines and block of gas engines and turbines used in the processing of the product gas (biomass gasification). For this purpose, in situ gas purification is one of the major issues nowadays related to practical biomass gasification in order to improve the viability and efficiency of the process [10,13,14]. Steam is the mainly used gasification medium leading to a product gas with high percentage of di-hydrogen [13,15]. The addition of steam has been reported to form fewer refractory tars, enhance phenol production that can be easier reformed catalytically, and eliminate the concentration of other oxygenates [13,16–18]. When a wood-biomass gasification process is used phenol can be a representative model compound of tar [3,17].

A large number of catalysts have been tested with significant ability for tar decomposition in various gasifier streams [7,10,16].

* Corresponding author. Tel.: +357 22 892776; fax: +357 22 892801.
E-mail address: efstath@ucy.ac.cy (A.M. Efstathiou).

These catalysts include sodium and potassium carbonates, metal oxides (e.g. $Al_2O_3$, $ZrO_2$, $CeO_2$ and calcined dolomites) and supported-metal oxides (e.g. $Ni/Al_2O_3$, $Rh/CeO_2$ and $Rh/ZrO_2$). Regarding the latter group, supported-Ni catalysts are in general the most frequently used industrial catalysts for gasification/reforming reactions of aromatics. In particular, Ni-based catalysts were found to be effective for tar destruction producing high yields of synthesis gas [19,20]. Due to their low attrition resistance, these catalysts are generally placed downstream the gasifier in a separate fixed-bed reactor [20,21]. Another limitation of Ni-based catalysts is the built-up of surface carbon deposits that leads to rapid deactivation and limited catalyst life-time [21–24].

The ability of using metal oxides and specifically those derived from natural materials appears to be more advantageous compared to Ni-based catalysts for fluidized-bed reactor applications, where the loss of catalytic material is not negligible [10,16,17]. Calcined dolomites $(CaMg(CO_3)_2)$, olivines $((Mg,Fe)_2SiO_4)$, and calcites $(CaCO_3)$ can be attractive "in bed" materials because they are inexpensive, non-toxic and disposable, and can be also significantly active at high temperatures [15–29]. Extensive studies conducted by several research groups led to the conclusion that dolomites are very effective tar reforming catalysts [26,27,30–32] with the only problem being the continuous deterioration of their mechanical strength over reaction time [31,32]. In addition, olivines were found to exhibit comparable activity to calcined dolomites towards reforming reactions, and higher attrition resistance [21,28,29,33]. To our knowledge, a very limited number of published works was reported on the steam reforming of tar compounds using natural calcite materials [26,27,34–36]. The use of the latter materials in fluidized-bed reactor configurations can be very promising for the conversion of biomass with steam into a product gas of high $H_2$-yield. In particular, the process can be more efficient than the conventional gasification method due to the in situ integration of the reaction heats of $CO_2$ absorption and water–gas shift reaction into the gasification/reforming reaction network, resulting to a product gas with high hydrogen and low CO content [17,37–39].

The present work is focused on some detailed catalytic study of the steam reforming of phenol towards hydrogen production in a fixed-bed micro-reactor over a natural calcite material in the 650–800 °C range. The latter material was identified as the best solid over a series of natural calcite materials of different geographical origin [40]. The selection of phenol as a model compound of tar was based on experimental results of steam gasification of wood-biomass in a fast-recycled fluidized-bed reactor in which phenol was reported to be one of the major tar constituents [17]. The present work provides substantial and important fundamental information on the effects of (a) reaction temperature, (b) water feed concentration, (c) gas hourly space velocity (GHSV, $h^{-1}$), and (d) the presence of $H_2$ and $CO_2$ in the feed stream on the rate of reaction at hand. Furthermore, cycle-stability experiments, carbon accumulation measurements, $CO_2$ temperature-programmed desorption (TPD), and in situ diffuse reflectance infrared Fourier transform spectroscopy (DRIFTS)-$CO_2$ chemisorption under various gas atmospheres were conducted for better understanding of the present catalytic reaction system.

## 2. Experimental

### 2.1. Catalyst characterization

#### 2.1.1. Catalyst texture
The specific surface area ($m^2/g$), the pore volume ($cm^3/g$), and the average pore diameter (nm) of the natural calcite material investigated were determined by $N_2$ adsorption at 77 K using a Micromeritics Gemini III Surface Area and Pore Size Analyzer. In situ outgassing of the sample (as received or followed calcination in air at

850 °C for 2 h) at 200 °C for 4 h under vacuum ($P \approx 1.3 \times 10^{-3}$) was performed before measurements were taken.

#### 2.1.2. X-ray diffraction studies
The mean primary crystallite size ($d_c$, nm) of the raw natural calcite material and that resulted after its calcination in air at 850 °C for 2 h was estimated from powder X-ray diffraction (XRD) measurements (Shimadzu 6000 diffractometer, Cu $K_{\alpha}$ radiation ($\lambda$ = 1.5418 Å)) and after using the Scherrer equation [41]. The sample of the natural calcite material used was crushed and sieved to lower than 200 mesh size before measurements. The diffractograms were taken in the range of $2\theta$ between 10° and 80° with a step of 2°/min.

#### 2.1.3. HRTEM and EDX spectroscopy studies
The morphology of the natural calcite material was examined by high resolution transmission electron microscopy (HRTEM) using a JEOL 2100F transmission electron microscope with a field emission gun (FEG) and a point resolution of 0.19 nm. The elemental chemical analysis of the natural calcite material was performed using the energy dispersive X-ray (EDX) thin-window in the spectrometer (INCA x-sight, Oxford Instrument) which was coupled with the TEM microscope. The weight % and atom % compositions of the sample were determined by the provided instrument's software and appropriate calibration procedures. The specimen was prepared by ultrasonically dispersing the powder sample in iso-octane and placing a droplet of the suspension on a copper grid covered with a carbon film.
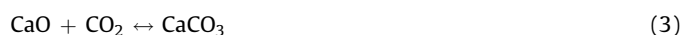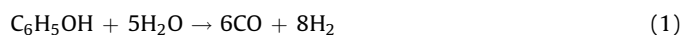
#### 2.1.4. $CO_2$ temperature-programmed desorption ($CO_2$-TPD)
$CO_2$ temperature-programmed desorption experiments were conducted in a specially designed gas-flow system previously described [42]. The fresh solid sample (0.5 g) was first calcined in 20%$O_2$/He at 850 °C for 2 h, purged in He and then cooled quickly to room temperature. The feed was subsequently switched to x vol%$CO_2$/He (x = 2 or 10) gas mixture for 30 min. Following this adsorption step the gas-flow was switched to He (30 N mL/min) for 15 min, where after this time no signal of $CO_2$ was detected in the mass spectrometer (Balzers, Omnistar). The temperature of the solid was then increased to 800 °C at the heating rate of $\beta$ = 30 °C/min. Calibration of the $CO_2$ signal at the mass to charge ratio, $m/z$ = 44 in the mass spectrometer was made based on a 1 vol% $CO_2$/He gas mixture.

### 2.2. Catalytic activity studies

The experimental apparatus used for catalytic measurements regarding the steam reforming of phenol reaction at 1 atm total pressure over the natural calcite material was described in detail elsewhere [43]. A 0.3-g sample of the natural calcite material ($d_p$ = 0.1–0.3 mm) was loaded in the micro-reactor. The total flow rate used was 200 N mL/min (GHSV $\approx$ 54,000 $h^{-1}$) and the feed gas consisted of 0.6%$C_6H_5OH$/40%$H_2O$/59.4%He, similar with respect to phenol and water composition to that encountered at the inlet (bottom) of the fluidized-bed used in the steam gasification of wood-biomass [17]. Initially, the catalyst sample was calcined in 20%$O_2$/80%He gas mixture at 850 °C for 2 h.

The steam reforming of phenol over a CaO-containing material can be described by the following reaction network [19,37,38,43–45]:

$$C_6H_5OH + 5H_2O \rightarrow 6CO + 8H_2 \tag{1}$$

$$CO + H_2O \leftrightarrow CO_2 + H_2 \tag{2}$$

$$CaO + CO_2 \leftrightarrow CaCO_3 \tag{3}$$

The most important parameters for catalyst evaluation in the present work are considered the conversion of phenol ($X_p$, %) and the selectivity of reaction towards hydrogen ($S_{H_2}$, %), according to the following relationships:

$$X_p (\%) = (F_{CO}^{exp} + F_{CO_2}^{exp})/6F_p^{in} \times 100 \qquad (4)$$

$$S_{H_2} (\%) = y_{H_2}^{out}/y_{H_2}^{max} \times 100 \qquad (5)$$

where, $F_{CO}^{exp}$ and $F_{CO_2}^{exp}$ are the experimental molar flow rates (mol/s) of CO and $CO_2$, respectively, $F_p^{in}$ is the molar flow rate of phenol in the feed stream (mol/s), $y_{H_2}^{out}$ is the mole fraction of $H_2$ in the outlet stream, and $y_{H_2}^{max}$ is the maximum production of $H_2$ (mole fraction) to be obtained considering 100% conversion for the steam reforming and water–gas shift reactions (Eqs. (1) and (2)). Eq. (4) was derived after applying appropriate mass balances. It should be noted that only very small concentrations of benzene and methane were experimentally observed in the product gas stream, and these are not included in Eq. (4).

The catalytic performance of the pre-calcined natural calcite material was studied in the 650–800 °C range. The effect of $H_2O$ (40 and 50 vol%), $H_2$ (15 and 30 vol%), and $CO_2$ (2, 5 and 10 vol%) in the feed stream, and of GHSV (30,000–85,000 $h^{-1}$) on the phenol conversion, $H_2$-selectivity, $H_2$-yield, and the $CO/CO_2$ product ratio were investigated. Catalytic measurements were taken after 20 min on stream at a given reaction temperature, where steady-state in the reaction rate was observed. The catalytic performance of CaO at this relatively short time on stream was of particular interest in the present work, where CaO is used in biomass gasification applications with fluidised-bed reactor configurations, where internal fast recycling of bed material from the reaction to the combustion zone is applied [17]. The latter is necessary for the regeneration of calcite (removal of carbonaceous deposits and conversion of $CaCO_3$ into CaO). It is also noted that between successive catalytic measurements (e.g. different reaction $T$ or feed gas composition) the catalyst sample was pre-treated in $20\%O_2/80\%He$ at 850 °C for 2 h.

## 2.3. Carbon deposition

The amount of carbonaceous species accumulated on the surface of CaO under reaction conditions was measured at a given reaction temperature and short time on stream for the reason given in the previous section. Following reaction with $0.6\%C_6H_5OH/40\%H_2O/He$ at 650 and 800 °C for 5 and 20 min, the feed was changed to He until the CO ($m/z = 28$) and $CO_2$ ($m/z = 44$) mass spectrometer signals reached their respective baseline value. The gas-flow was then switched to $20\%O_2/He$ and the transient signals of CO and $CO_2$ were continuously followed by *on line* mass spectrometry. The amount of surface "carbonaceous" deposits (g C/g catalyst) was calculated based on the CO and $CO_2$ transient response curves calibrated against standard mixtures and the appropriate carbon mass balance for a flow-reactor.

## 2.4. Isothermal adsorption of $CO_2$

The amount of carbon dioxide adsorbed on CaO (after calcination of the natural calcite material) was measured according to the following procedure. A 0.5-g sample of calcite material was initially pre-calcined in $20\%O_2/He$ for 2 h at 850 °C. The solid was then purged in He flow, cooled to 650 °C, and the gas-flow was subsequently switched to a $x\%CO_2/x\%Ar/He$ ($x = 2$ or 10) gas mixture (100 N mL/min). The presence of Ar in the adsorbing gas mixture served to record the reference transient response curve of a non-adsorbing and non-reacting gas (Ar) that passes from the

switching valve through the reactor to the mass spectrometer, step necessary for the quantitative estimation of adsorbed $CO_2$ [46].

## 2.5. In situ DRIFTS studies

*In situ* DRIFTS-$CO_2$ chemisorption studies were conducted on a PerkinElmer Spectrum GX II FTIR spectrometer equipped with a high-temperature/high-pressure controllable DRIFTS cell (Harrick, Praying Mantis). About 30 mg of the calcite material (pre-calcined *ex-situ* at 850 °C in air for 2 h) in a fine powder form were placed firmly into the ceramic cup of the DRIFTS cell. Chemisorption was performed using a $2\%CO_2/98\%He$ gas mixture (50 N mL/min) at 25 and 600 °C, and a $2\%CO_2/40\%H_2O/x\% H_2/He$ ($x = 0$, 30 and 50) gas mixture (100 N mL/min) at 600 °C. In each case of use of the latter adsorption gas mixture, a new fresh CaO sample was used which was pre-calcined *ex-situ* as mentioned above. Before any DRIFTS spectrum was recorded, the sample was also pretreated *in situ* in $20\%O_2/80\%Ar$ at 600 °C for 2 h. Signal averaging was set to 50 scans per spectrum at a 2 $cm^{-1}$ spectra resolution in the 4000–400 $cm^{-1}$ range.

DRIFTS-$CO_2$-TPD was performed following a 30 min gas adsorption at 25 °C under $2\%CO_2/98\%He$ gas mixture. The DRIFTS cell was then purged in Ar flow for 15 min and the temperature was then increased to 600 °C. DRIFTS spectra were recorded every 100 °C. Each DRIFTS spectrum presented here corresponds only to the spectrum of the adsorbed phase after subtracting the spectrum of the solid itself which was taken in Ar flow at the desired temperature. DRIFTS spectra when necessary were smoothed in order to remove high frequency noise and further analyzed using the software Spectrum for Windows. Deconvolution and curve fitting procedures of the DRIFTS spectra were performed according to reported guidelines and after using Gausian peak line shapes [47].

# 3. Results and discussion

## 3.1. Catalyst characterization

### 3.1.1. Catalyst texture, XRD and XPS studies

The specific surface area (BET, $m^2/g$), the pore volume ($cm^3/g$), and the average pore diameter (nm) of the natural calcite material as received ($CaCO_3$) and after calcination (CaO) [40] are listed in Table 1. The BET area and the pore volume of the calcite material outgassed at 200 °C under vacuum was found to increase upon calcination in air at 850 °C for 2 h. The opposite trend was observed for the pore diameter (Table 1). The above results are in agreement with those reported in the literature [48,49].

The XRD studies performed over the raw (as received) natural calcite material and that after calcination at 850 °C for 2 h revealed the structures of $CaCO_3$ and CaO (cubic structure), respectively [40]. The conversion of calcite material ($CaCO_3$) into calcium oxide (CaO) was also proven by DRIFTS experiments, where after calcination the main infrared bands due to the fundamental vibrational modes of $CO_3^{2-}$ were absent compared to the spectra recorded before calcination [40]. After using the Scherrer equation the estimated mean primary crystal size of the raw natural calcite

**Table 1**
Textural and mean primary crystal size characteristics of the natural calcite material outgassed at 200 °C under vacuum for 4 h and after calcination in air at 850 °C for 2 h.

| Physical properties | Before calcination (200 °C) | After calcinations (850 °C) |
|---|---|---|
| BET ($m^2/g$) | 0.4 | 8.0 |
| Pore volume ($cm^3/g$) | 0.001 | 0.019 |
| Average pore diameter (nm) | 14.4 | 7.5 |
| Mean primary crystal size (nm) | 40 | 51 |

**Table 2**
Elemental chemical analysis of the natural calcite material obtained by energy dispersive X-ray analysis.

| Element | wt% | at% |
|---------|------|------|
| Ca | 48.3 | 25.8 |
| O | 31.6 | 42.3 |
| C | 17.3 | 30.9 |
| Mg | 0.4 | 0.38 |
| Si | 0.09 | 0.08 |
| Sn | 0.8 | 0.16 |
| Sb | 1.5 | 0.3 |

material was found to increase following calcination (CaO phase, Table 1). The fact that the natural calcite material studied shows a high surface concentration of Ca and very low surface concentrations of metal impurities ($<0.4$ at%, Table 2) was also clearly revealed from X-ray photoelectron spectroscopy measurements. The binding energies of Ca $2p_{3/2}$ (347.1 eV) and C 1s (289.7 eV) peaks recorded are characteristic of calcium carbonates [50]. From the peak intensities and atomic sensitivity factors, a surface molar ratio of $CO_3^{2-}/Ca = 1.14$ was obtained which agrees satisfactorily with the stoichiometric bulk ratio of $CaCO_3$. Some minor impurities of Si, Sb and Mg were also detected in harmony also with the bulk chemical analysis composition found (see Section 3.1.2).

All the above results imply that calcination of the natural calcite material in air at 850 °C for 2 h involves the decomposition of the carbonate mineral into CaO, the latter being the active phase responsible for the observed activity towards steam reforming of phenol.

### 3.1.2. EDX and HRTEM studies

Table 2 presents the elemental composition (wt% or at%) of the natural calcite as determined by EDX spectroscopy. The material contains small amounts ($<0.8$ wt%) of metal impurities (Mg, Si and Sn) with slightly larger Sb amounts (1.52 wt%). In terms of atom % composition, all metal impurity levels are significantly lower ($<0.4$ at%). These results are in harmony with the XRD measurements, where besides CaO no other metal oxide phases due to these metal impurities could be seen [40].

Fig. 1 shows HRTEM images obtained on the natural calcite material as received. At the lowest resolution (Fig. 1a, 200 nm scale unit; Fig. 1b, 100 nm scale unit), the sample appears as irregular particles formed from aggregates of randomly oriented smaller particles but with no defined crystal shape. At the highest resolution (Fig. 1c, 20 nm scale unit), aggregation of smaller particles is clearly visible although no well defined crystalline shape can be observed. In addition, some pores of irregular shape are discerned. It is important to note here that previous studies [40] on a series of natural calcite materials of different geographical origin with different morphological characteristics (SEM studies) and similar mean primary crystallite size ($d_c \sim 44$–$51$ nm, XRD studies) revealed that the phenol steam reforming specific reaction rate ($\mu$mol/m$^2$ min) is influenced by the surface morphology and defect structure of its primary crystals.

### 3.2. Catalytic performance of CaO derived from natural calcite

### 3.2.1. Effect of reaction temperature

The steam reforming of phenol towards hydrogen production was studied in the 650–800 °C range over a pre-calcined natural calcite material (in the form of CaO) as described in Section 2.2. Fig. 2a presents results of the effect of reaction temperature on phenol conversion, $X_P$ (%) and the specific rate of phenol conversion, $R_P$ ($\mu$mol $C_6H_5OH/m^2$ min) both estimated based on the experimental CO and $CO_2$ product concentrations (see Section 2.2) after steady-state was achieved. It is seen that the activity of
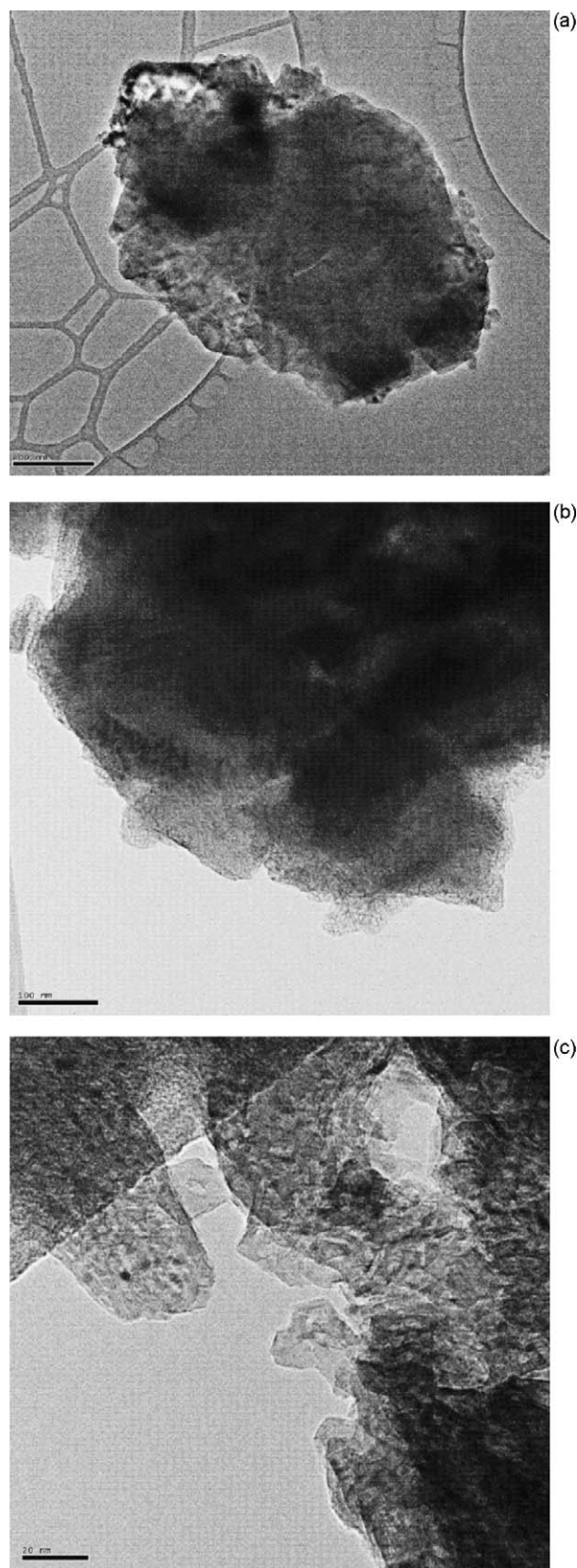
**Fig. 1.** TEM images of the raw natural calcite material at different magnifications. Scale unit in each photo is as follows: (a) 200 nm; (b) 100 nm; (c) 20 nm.
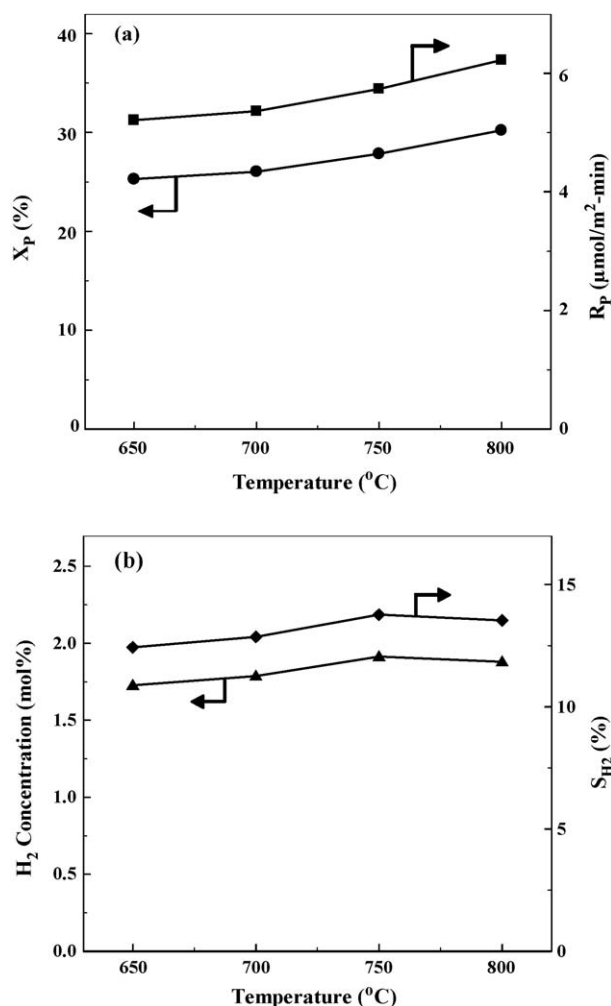
**Fig. 2.** Dependence of (a) phenol conversion ($X_P$, %) and specific rate of phenol conversion ($R_P$, μmol $C_6H_5OH$/($m^2$ min)), and (b) $H_2$ product concentration (mol%, dry basis) and hydrogen selectivity ($S_{H_2}$, %) on reaction temperature over the natural calcite material. Feed composition used: $0.6\%C_6H_5OH/40\%H_2O/59.4\%He$; $W_{cat}$ = 0.3 g; $F_T$ = 200 mL/min.

CaO in terms of phenol conversion and specific reaction rate slightly increase with reaction temperature in the 650–800 °C range. An increase by 20% in $X_p$ was observed after increasing the reaction temperature from 650 to 800 °C. Fig. 2b presents results of the $H_2$ product concentration (mol%, dry basis) and $H_2$-selectivity ($S_{H_2}$, %) obtained in the 650–800 °C range. These results show that both the hydrogen yield and hydrogen selectivity are also slightly affected by the reaction temperature, where maximum $H_2$-yield seems to occur at 750 °C. It is important to note that the maximum theoretical $H_2$ concentration (mol%) expected according to the network of reactions (1) and (2), the feed gas composition used, and considering 100% phenol conversion is 13.9 mol%. Based on the results of Fig. 2, it is seen that the investigated natural CaO (Table 1) appears to present not significant activity under the GHSV ($\sim$54,000 $h^{-1}$) and reaction temperature ($T < 700$ °C) of interest [17].

According to studies performed by Delgado et al. [26,27] on the use of dolomite, calcite and magnetite natural materials for the cleaning from tars of raw hot gas derived from biomass gasifiers with steam, the hydrogen yield was found to increase with reaction temperature, and significant values at temperatures higher than 840 °C were achieved. In addition, over calcite and magnetite materials a clean gas from tars could be obtained when using lower space velocities [26] than what used in the present work.

Moreover, Simell et al. [36] in an attempt to decompose tarry constituents in flue gas using low-cost materials (dolomite, limestone), complete tar decomposition (especially consisted of benzene) was accomplished at 900 °C. Furthermore, Garcia et al. [35] after studying the catalytic steam gasification of three tars from different sources (e.g. oil refinery, coal gasification) using CaO (fixed-bed reactor), the latter derived following limestone calcination, it was reported that steam-to-tar ratio is an important parameter for complete conversion of tars to gaseous products. A steam-to-tar ratio of 3.5 and temperatures higher than 750 °C were found to lead to complete conversion of tars to gaseous products due to the higher gasification rate compared to the solid carbon generation rate obtained.

### 3.2.2. Effect of water composition in the feed stream

The effect of water feed concentration on the hydrogen selectivity ($S_{H_2}$, %) and $CO/CO_2$ product ratio in the 650–800 °C range is presented in Fig. 3a and Fig. 3b, respectively. The phenol feed concentration (0.6 vol%) and GHSV ($\sim$54,000 $h^{-1}$) were kept constant, while the water concentration was varied in the 40–50 vol% range. It is observed that $S_{H_2}$ (%) increases with increasing concentration of water in the feed stream in the whole 650–800 °C range (Fig. 3a). At 650 °C, an increase by 22% in $S_{H_2}$ was seen after
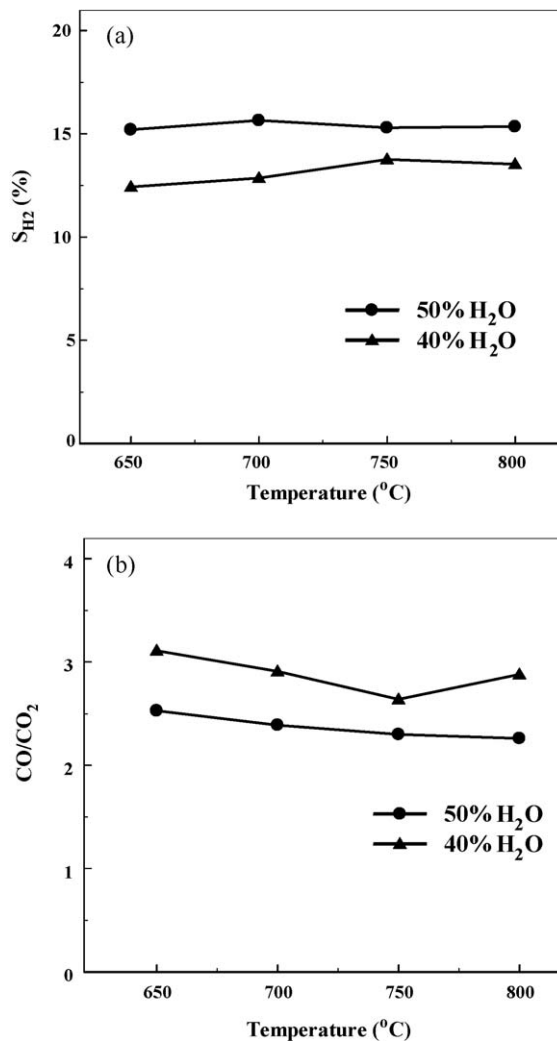


**Fig. 3.** Dependence of (a) hydrogen selectivity ($S_{H_2}$, %) and (b) $CO/CO_2$ product ratio on reaction temperature and water feed concentration for the natural calcite material. Feed composition used: $0.6\%C_6H_5OH/x\%H_2O/He$, $x$ = 40 or 50; $W_{cat}$ = 0.3 g; $F_T$ = 200 mL/min.

increasing the water feed concentration from 40 to 50 vol%. This result illustrates that the increase of water concentration is beneficial for both reactions (1) and (2) towards hydrogen production. No significant change in $S_{H_2}$ with reaction temperature was observed under both water feed concentrations. This can be understood by the relatively small change in phenol conversion with reaction temperature (Fig. 2a), and the negative effect of reaction $T$ on the hydrogen production via the water–gas shift reaction (exothermic). For the latter, the increase of decomposition rate of $CaCO_3$ to CaO and $CO_2$ (Eq. (3)) and the negative influence of produced $CO_2$ on $H_2$ production via the water–gas shift reaction (Eq. (2)) is another factor that influences $S_{H_2}$ behavior with reaction $T$.

On the other hand, the $CO/CO_2$ product ratio decreases with increasing $H_2O$ feed concentration (Fig. 3b), further indicating the promotion of the water–gas shift reaction (2). The $CO/CO_2$ product ratio versus the reaction temperature profile seems to depend on the feed water concentration. These results are in harmony with the fact that water enhances the cracking efficiencies of aromatic components to be reformed [51], thus increasing $S_{H_2}$ and carbon dioxide formation [52]. In addition, water is essential for the steam reforming of oxygenated aromatics that require a high steam-to-carbon ratio in order to suppress formation of coke on the catalyst surface [19].

### 3.2.3. Effect of hydrogen in the feed stream

Fig. 4 presents the effect of hydrogen feed concentration on phenol conversion, $X_p$ (%) (Fig. 4a) and $CO/CO_2$ product ratio (Fig. 4b) obtained over the natural pre-calcined calcite material in the 650–800 °C range. The phenol and water concentrations were kept constant at 0.6 and 40 vol%, respectively (GHSV = ~54,000 h$^{-1}$). As shown in Fig. 4a, the increase of $H_2$ concentration in the feed stream from 0 to 30 vol% results in a significant decrease of phenol conversion at all the reaction temperatures studied. In particular, phenol conversion decreased by approximately 50% in the presence of 30 vol% $H_2$ in the feed stream in the low 650–700 °C range. This caused the water–gas shift reaction (2) to shift to lower hydrogen production, and, therefore, to higher $CO/CO_2$ product ratios (Fig. 4b). While a similar effect on $X_p$ (%) is observed at 650 °C when 15 vol% compared to 30 vol% $H_2$ is used in the feed, this effect becomes smaller at higher reaction temperatures (Fig. 4a).

A very similar behavior of activity decrease with increasing $H_2$ feed concentration from 0 to 30 vol% (Fig. 4a) was also obtained with the presence of 50 vol% $H_2$ in the feed stream. The experimental results of Fig. 4 illustrate the strong suppressing effect of hydrogen towards phenol steam reforming activity, implying that the reaction order with respect to $H_2$ is negative for either the reforming reaction (1) or the water–gas shift reaction (2), or both reactions.

It has been reported that hydrogen is dissociatively adsorbed on MgO and other metal oxide surfaces with the metal cation–oxygen anion pairs being the active sites of adsorption [53,54]. According to this, hydrogen is adsorbed on the $O^{n-}$ anions of CaO surface via heterolytic dissociation, blocking, therefore, active sites of the surface essential for decomposition and further reaction steps necessary for reactions (1) and (2). This could appear as a main reason for the negative role of hydrogen presence in the reaction feed of phenol/water. In Sections 3.7.2 and 3.8 this hydrogen suppressing effect on phenol steam reforming activity is further discussed based on various DRIFTS chemisorption experiments performed. The negative effect of $H_2$ feed concentration towards steam reforming of model compounds of tar has also been reported by Taralas [52] for the catalytic steam reforming of $n$-heptane. The author observed that the yield of $CO_2$ was decreased with the addition of hydrogen over calcined
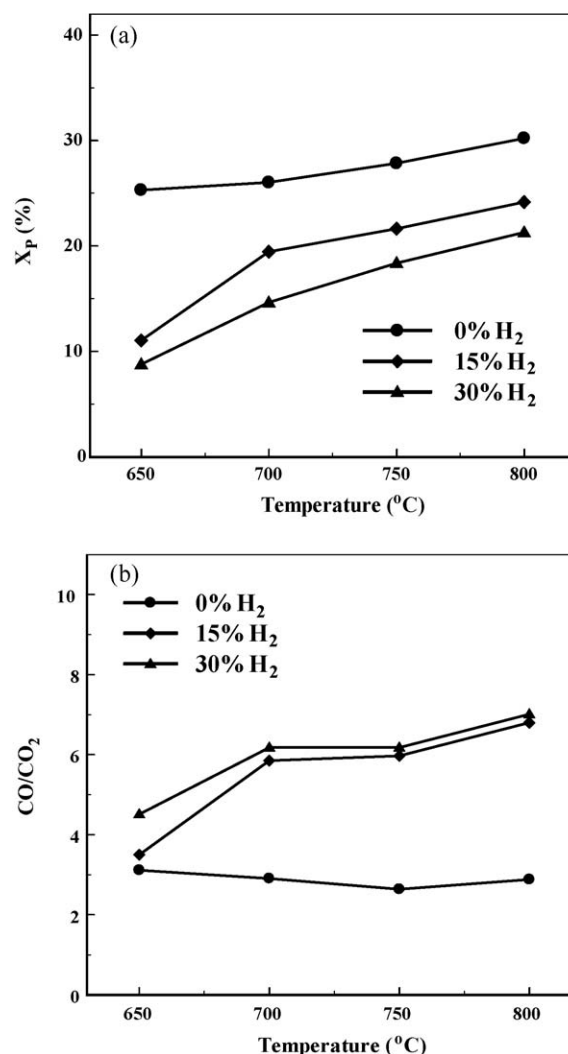


**Fig. 4.** Dependence of (a) phenol conversion ($X_p$, %) and (b) $CO/CO_2$ product ratio on reaction temperature and hydrogen feed concentration for the natural calcite material. Feed composition used: $0.6\%C_6H_5OH/40\%H_2O/x\%H_2/He$, $x$ = 0, 15 or 30; $W_{cat}$ = 0.3 g; $F_T$ = 200 mL/min.

dolomite, suggesting the suppression of reactions (1) and (2). In addition, Aldén et al. [51] investigated the influence of gas components on naphthalene decomposition over calcined dolomite, where $H_2$ was found to be a strong inhibitor of the reaction rate. Simell et al. [55,56] have studied benzene and toluene decomposition over calcined dolomite and found that hydrogen was dissociatively adsorbed onto the active sites (e.g. $Mg^{2+}$–$O^{2-}$ and $Ca^{2+}$–$O^2$), thus lowering the decomposition rate of benzene and toluene. Furthermore, experimental studies on the non-catalytic steam reforming decomposition of toluene, benzene and naphthalene showed that the presence of $H_2$ in the feed stream led to a decrease in the formation of CO with a negative effect on the corresponding steam reforming activity [57,58].

The effect of $H_2$ concentration (0–30 vol%) on the phenol conversion, $X_p$ (%) was also investigated with higher water concentrations (e.g. 50 vol%) in the feed stream; the phenol concentration was kept constant at 0.6 vol%. Fig. 5 shows that by increasing the hydrogen feed concentration from 0 to 30 vol% leads to a gradual decrease of phenol conversion at all reaction temperatures (650–800 °C), in particular in the 650–700 °C range, result similar to that reported in Fig. 4a after using 40 vol% water in the feed stream. However, the negative effect of the presence of $H_2$ in the feed stream on phenol steam reforming activity over CaO is
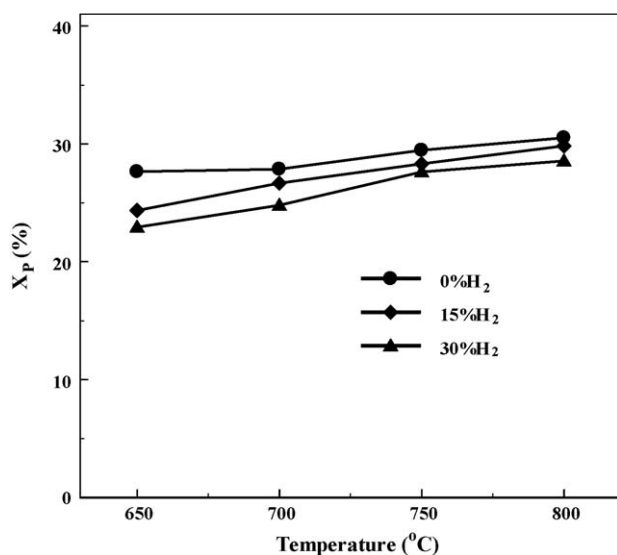
Fig. 5. Dependence of phenol conversion ($X_p$, %) on reaction temperature and hydrogen concentration in the feed stream for the natural calcite material. Feed composition used: $0.6\%C_6H_5OH/50\%H_2O/x\%H_2/He$, $x = 0$, 15 or 30; $W_{cat} = 0.3$ g; $F_T = 200$ mL/min.

smaller when 50 vol% than 40 vol% $H_2O$ in the feed stream is used. As will be discussed in Section 3.7, water and hydrogen molecules compete for the same adsorption sites. The rate of this competitive chemisorption is expected to be governed by a different kinetics, the latter depending on the concentration of $H_2$ or $H_2O$, explaining, therefore the results of Figs. 4a and 5.

### 3.2.4. Effect of gas hourly space velocity (GHSV, $h^{-1}$)

Fig. 6 shows the effect of gas hourly space velocity on phenol conversion, $X_p$ (%) and hydrogen selectivity, $S_{H_2}$ (%) obtained over CaO at 650 and 750 °C. It is clearly seen that both catalyst performance parameters decreased with increasing GHSV from 30,000 to 80,000 $h^{-1}$. In particular, at 750 °C about 30% decrease in phenol conversion and $H_2$-selectivity was obtained. Moreover, the phenol conversion and $H_2$-selectivity both increase with increasing reaction temperature (650–750 °C) as also shown in Fig. 2a and b. The increase of $H_2$-yield and $H_2$-selectivity with decreasing GHSV ($h^{-1}$) has also been reported [19,59].
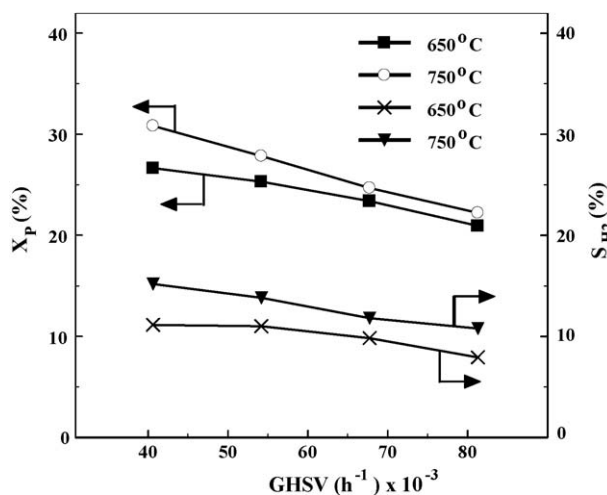


Fig. 6. Dependence of phenol conversion ($X_p$, %) and hydrogen selectivity ($S_{H_2}$, %) on gas hourly space velocity (GHSV, $h^{-1}$) and reaction temperature for the natural calcite material. Feed composition used: $0.6\%C_6H_5OH/40\%H_2O/59.4\%He$; $W_{cat} = 0.3$ g.
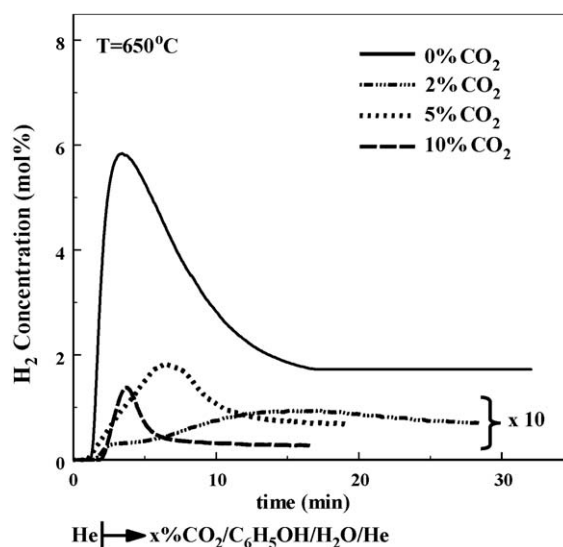


Fig. 7. Dependence of $H_2$ product concentration (vol%) on carbon dioxide feed concentration at 650 °C for the natural calcite material. Feed composition used: $0.6\%C_6H_5OH/40\%H_2O/x\%CO_2/He$, $x = 0$, 2, 5 or 10; $W_{cat} = 0.3$ g; $F_T = 200$ mL/min.

### 3.2.5. Effect of carbon dioxide in the feed stream

Fig. 7 compares the transient isothermal ($T = 650$ °C) evolution of hydrogen product concentration in the case when carbon dioxide was added in the feed stream (2–10 vol%); the phenol and water concentrations were 0.6 and 40 vol%, respectively. By increasing the feed concentration of $CO_2$ in the 0–10 vol% range, the pseudo-steady-state concentration of hydrogen produced is significantly decreased (see Fig. 7 for $t > 15$ min), and more remarkably the initial reaction rate; compare the feature of sharp appearance of rate maximum obtained with 0 vol% $CO_2$ which vanishes at higher $CO_2$ feed concentrations. Furthermore, after about 1 h treatment of CaO with $10\%CO_2/He$, the activity of the solid drops to zero, the case of the natural calcite material as received.

The same trend was also observed at 700 °C with the effect of $CO_2$ on $H_2$ product concentration to be more intense at 650 °C. The possibility of having dry-reforming of methane in the presence of 2, 5 and 10 vol% $CO_2$ was investigated due to some small amounts of $CH_4$ measured during the steam reforming of phenol (0 vol% $CO_2$ in the feed). The latter investigation led to the observation that the hydrogen concentration produced was too low compared to that reported in Fig. 7, concluding, therefore, that dry-reforming of methane does not contribute to the transient activity results observed (Fig. 7). The results of Fig. 7 are consistent to the facts that the increase of $CO_2$ in the feed stream should cause the water–gas shift reaction (2) to shift to lower $H_2$ product concentrations, and that $CO_2$ poisons active basic catalytic sites of the CaO surface essential for the decomposition/reaction of phenol and water. The results of Fig. 7 demonstrate the inhibiting effect of the presence of $CO_2$ in the feed stream on steam reforming of phenol activity, as it is also observed with $H_2$ (Figs. 4a, b and 5).

An interesting kinetic feature of the $H_2$ transient response curves shown in Fig. 7 is the fact that the time evolution of the maximum $H_2$ concentration formed, as reflected by the maximum reaction rate, shifts to lower reaction times with increasing $CO_2$ concentration in the feed stream. On the other hand, at the highest $CO_2$ concentration used (10 vol%) there is a small delay in the appearance of $CO_2$ with the transient curve having essentially all the characteristic features (position and shape) of that obtained when no $CO_2$ in the feed stream was present. It is out of the scope of the present work to describe in detail these hydrogen dynamic responses based on kinetic model(s). What is important from these

transient response curves is the fact that the reaction rate of phenol steam reforming is kinetically influenced by the adsorption of $CO_2$ on the CaO surface, forming various kinds of carbonate species (see Section 3.7), and it is not simply influenced only by the reduction in the number of active sites (poisoning effect) present on the CaO surface. It seems that at a given range of $CO_2$ concentrations in the feed both the above-mentioned parameters affect the kinetics of phenol steam reforming.

The inhibiting effect of carbon dioxide in the decomposition of tars by steam was also reported in the literature [52,56,60]. The influence of carbon dioxide in the steam cracking of n-heptane was investigated over a calcined dolomite [52], where a decrease in n-heptane conversion and hydrogen yield were observed. Moreover, the rate-retarding effect of $CO_2$ was also reported in the steam gasification of naphthalene and toluene over calcined limestone and dolomite, respectively [56,60]. This effect was assumed to be due to the blocking of active sites on CaO by adsorbed $CO_2$, leading to the formation of calcium carbonate [56,61]. It was also reported that the rate of steam reforming is inversely proportional to the partial pressure of $CO_2$ [56].

Based on all the above experimental evidence, the activity of calcined calcites and dolomites must take the lowest value when the $CO_2$ partial pressure in the feed stream becomes greater than the equilibrium decomposition pressure of $CaCO_3$ and $MgCO_3$ [10,39,62]. According to the equilibrium decomposition curve of $CaCO_3$ [39,62], and the experimental conditions used in the present work (Fig. 7), the equilibrium decomposition pressure of $CaCO_3$ at 650 °C is about 1 kPa (1 vol% $CO_2$). Consequently, the CaO is expected to be found in a carbonated form ($CaCO_3$) since the $CO_2$ partial pressure used in the present experiments was greater than 1 vol%. In the case where the experimental process was performed at 700 °C, the decrease of hydrogen product concentration was significantly higher only when the $CO_2$ present in the feed was larger than 5 vol%.

### 3.3. Catalyst stability under alternating gas composition

The use of CaO-containing materials for tar destruction is related to the absorption enhanced reforming (AER) process [17,63], where the loaded catalytic/$CO_2$-absorbent bed material is circulated between two fluidised-bed reactors, taking up $CO_2$ in the reactor zone and regenerated by releasing the $CO_2$ and carbon deposits in the fluidised-bed combustor. Thus, the cycle stability is a crucial issue in this AER process to be investigated under consecutive oxidation/reaction cycles. The reaction step was performed for 10 min at 680 °C with a feed gas mixture consisting of 0.6%$C_6H_5OH$/40%$H_2O$/30%$H_2$/He, while the oxidation step (calcination) was performed with 2%$CO_2$/12%$H_2O$/2%$O_2$/$N_2$ for 5 min at 850 °C similar to the reaction and combustion mixtures encountered at the inlet of the fluidized-bed and combustor reactor, respectively, in a wood-biomass gasification process [17].

Fig. 8 compares the specific rate of phenol conversion, $R_P$ (μmol $C_6H_5OH$/($m^2$ min)) obtained after 10 consecutive oxidation/reaction cycles. The cycle numbered zero in Fig. 8 represents the initial activity of CaO before the first cycle was applied. It is observed that the activity decreases with increasing oxidation/reaction cycles. In particular, the initial activity dropped by about 40% after six consecutive cycles, where after that the catalytic activity remains practically the same, within 5%.

### 3.4. Characterization of carbonaceous species formed under steam reforming of phenol

The amount of carbonaceous species accumulated on the surface of CaO for short times on stream (up to 20 min) was measured following 0.6%$C_6H_5O$/40%$H_2O$/He reaction as described
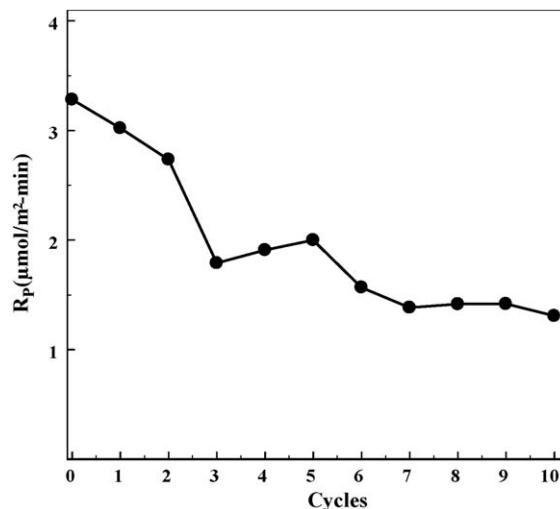


**Fig. 8.** Specific rate of phenol conversion ($R_P$, μmol $C_6H_5OH$/($m^2$ min)) obtained after consecutive oxidation → reaction cycles for short times at 680 °C over the natural calcite material. Reaction feed gas: 0.6%$C_6H_5OH$/40%$H_2O$/30%$H_2$/29.4%He for 10 min; oxidation step: 2%$CO_2$/12 %$H_2O$/2%$O_2$/84%$N_2$ at 800 °C for 5 min.

in Section 2.3. It is noted that the amount of "*carbonaceous*" species reflects the amount of "carbon-containing" intermediate species formed expressed as μmol C/g solid. It does not represent any specific chemical structure or composition of carbon. The amount of carbonaceous species was measured under the 20%$O_2$/80%He gas treatment of the solid with respect to the reaction temperature and time on stream. The experiments were performed at 650 and 800 °C for 5 and 20 min on stream.

Fig. 9 shows the transient response curves of $CO_2$ and CO obtained under the flow of 20%$O_2$/He gas mixture at 800 °C following a 20 min phenol steam reforming reaction over CaO. A large $CO_2$ (444 μmol/g) and a smaller CO peak (110 μmol/g) are obtained after a few minutes in the $O_2$/He gas stream. After about 10 min of oxidation reaction, a second small peak of $CO_2$ is formed, likely indicative of a second type of carbonaceous species less active towards oxidation. Table 3 provides the amount (μmol C/g $CaCO_3$, calcite sample before calcination) of accumulated carbo-
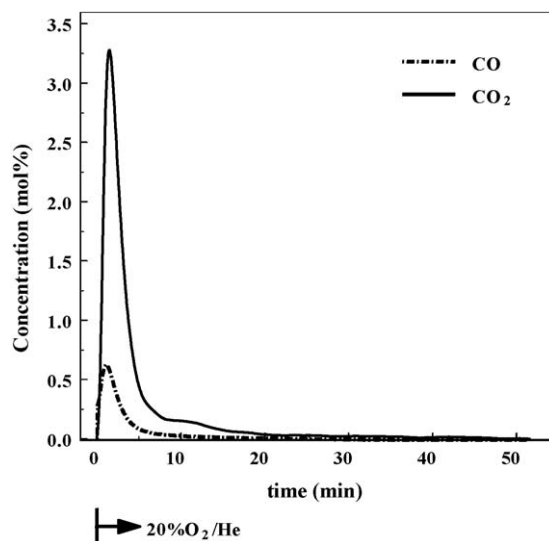


**Fig. 9.** Isothermal transient response curves of $CO_2$ and CO obtained in 20%$O_2$/He flow on the natural calcite material after steam reforming reaction of phenol at 800 °C for 20 min. Feed: 0.6%$C_6H_5OH$/40%$H_2O$/59.4%He; $W_{cat}$ = 0.3 g; $F_T$ = 200 mL/min.

**Table 3**
Amount ($\mu$mol C/g)[a] of carbonaceous species accumulated on the surface of CaO measured after $0.6\%C_6H_5O/40\%H_2O/He$ reaction as a function of reaction temperature and time on stream.

| Temperature (°C) | Time on stream (min) | $\mu$mol C/g |
|---|---|---|
| 650 | 5 | 532 (6.4)[b] |
|  | 20 | 583 (7.0) |
| 800 | 5 | 396 (4.7) |
|  | 20 | 555 (6.7) |

[a] Per gram of $CaCO_3$ (calcite sample before calcination).
[b] Number in parentheses represent mg C/g $CaCO_3$ (calcite sample before calcination).

naceous species with respect to reaction temperature and time on stream formed on the surface of CaO. It is seen that the amount of carbonaceous species increases with reaction time, especially at 800 °C. In addition, the amount of carbonaceous deposits is higher at the low reaction temperature of reforming. The amount of 583 $\mu$mol C/g (equivalent to 7 mg C/g) accumulated on the surface of the solid after 20 min on stream might be expected to be the highest accumulated amount since the steam reforming of phenol reached steady-state after about 20 min on stream. However, the latter may not be the case if accumulation of higher amounts of carbonaceous deposits does not hinder the main reforming reaction network occurred on CaO.

### 3.5. $CO_2$ chemisorption at 25 °C followed by TPD

$CO_2$ chemisorption experiments at 25 °C using $2\%CO_2/98\%He$ and $10\%CO_2/90\%He$ gas adsorption mixtures followed by TPD in He flow were conducted over CaO. Fig. 10 presents TPD response curves of $CO_2$, where of interest is the high temperature that $CO_2$ desorption was observed ($T > 500$ °C), confirming the high strength of basic sites of the CaO surface towards $CO_2$ in agreement with the literature [64]. As shown in Fig. 10, two distinct desorption peaks with peak maxima at 711 and 800 °C were obtained with a tail at the rising part of the low-$T$ peak, and a shoulder at the falling part of the high-$T$ desorption peak ($2\%CO_2/$He adsorption mixture). However, when a $10\%CO_2/He$ adsorption mixture was used only one smaller peak is emerged centered at 715 °C with a tail at the rising part of the peak. These results illustrate that at least two kinds of adsorbed carbonate species are formed on the surface of CaO in accordance to in situ DRIFTS studies
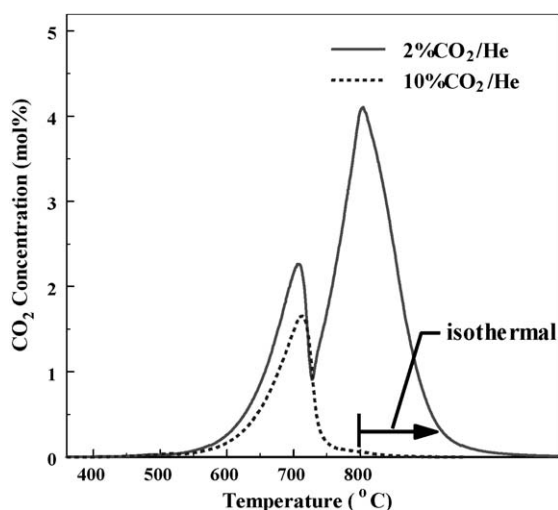


**Fig. 10.** Temperature-programmed desorption (TPD) response curves of $CO_2$ under He flow obtained over the natural calcite material. Adsorption conditions: $x\%CO_2/He$ ($x$ = 2 or 10), 25 °C, 30 min. Desorption conditions: $Q_{He}$ = 30 N mL/min, $\beta$ = 30 °C/min.

(see Section 3.7). Also, these results indicate that carbonation of CaO takes place in the surface/subsurface region (low-$T$ desorption peak) and in the bulk (high-$T$ desorption peak) of the solid [56,61,62]. It is obvious that decomposition of surface carbonates formed is much easier than that of bulk carbonates. This supports the view that formation of more thermally stable bulk carbonates (desorbed at $T > 800$ °C) in the case of using a high $CO_2$ partial pressure ($10\%CO_2/He$) takes place as compared to the case of using a lower one.

The amount of $CO_2$ desorbed from the surface of CaO (up to 800 °C until no desorption of $CO_2$ was seen) was found to decrease with increasing concentration of $CO_2$ in the adsorption mixture. A value of 481 $\mu$mol/g or 60.1 $\mu$mol/m$^2$ was estimated when a $2\%CO_2/He$ gas mixture was used, which is by far larger than the value of 108.1 $\mu$mol/g or 13.5 $\mu$mol/m$^2$ obtained when a $10\%CO_2/$He gas mixture was used. This result is consistent to the fact that more stable bulk carbonates are formed in the case of exposure of the sample in high $CO_2$ partial pressures. The latter would also indicate that the rate of steam reforming depends inversely on the partial pressure of $CO_2$ in agreement to what reported [56] and also with the activity measurements performed here in the case where $CO_2$ was present in the feed stream (see Section 3.2.5).

### 3.6. Isothermal transient adsorption of $CO_2$

The $CO_2$ adsorption characteristics of the CaO surface have also been investigated through dynamic experiments after step concentration switches of the feed composition between $O_2/He$ and $CO_2/He$ (see Section 2.4.). Fig. 11 presents the evolution of transient gas-phase response curves of Ar and $CO_2$ concentration according to the sequence: $20\%O_2/He$ (800 °C, 2 h) $\rightarrow$ He (650 °C, 15 min) $\rightarrow$ $x\%CO_2/x\%Ar/He$ (650 °C, $t$), where $x$ corresponds to 2 vol% (Fig. 11a), or 10 vol% (Fig. 11b). The area difference between the Ar and $CO_2$ response curves provides the amount ($\mu$mol/g) of $CO_2$ adsorbed isothermally on the surface of CaO. In the case of Fig. 11a, this amount was found to be 8470 $\mu$mol/g, whereas in the case of Fig. 11b it was 6710 $\mu$mol/g. It is important to note that adsorption of $CO_2$ takes much longer (lasts nearly 3 h) after using $2\%CO_2/2\%Ar/He$ (Fig. 11a) compared to the case of $10\%CO_2/10\%Ar/$He (lasts about 25 min, Fig. 11b). This difference is strongly related to the mechanism of surface and bulk carbonation of CaO, where for the latter case a slow diffusion of $CO_2$ takes place through a crust of $CaCO_3$ formed.

The comparison of Figs. 10 and 11 shows the dependency of the $CO_2$ adsorption capacity of CaO on the concentration and temperature of exposure to $CO_2$. As clearly seen the $CO_2$ adsorption capacity increases with increasing $CO_2$ exposure temperature, in agreement to what reported previously [61]. This result is also in harmony with in situ DRIFTS studies (see Section 3.7), where the surface concentration of carbonates was found to be larger at 600 °C compared to 25 °C.

### 3.7. In situ DRIFTS

#### 3.7.1. Chemical structure and thermal stability of adsorbed surface carbonates ($CO_2/Ar$ treatment)
The chemical structure of adsorbed carbonate species formed on the surface of the pre-calcined natural calcite material (CaO) was investigated by in situ DRIFTS-$CO_2$ chemisorption and desorption studies under various gas atmospheres. Fig. 12a compares the DRIFTS spectra recorded in the 1800–1100 cm$^{-1}$ range after heating CaO to 100, 300 and 600 °C under Ar gas-flow following exposure of the CaO surface to a $2\%CO_2/Ar$ gas mixture at room temperature for 30 min. After deconvolution of the spectral region 1800–1500 cm$^{-1}$ recorded at 100 °C, the IR band centered at 1750 cm$^{-1}$ can be assigned to the C–O stretching vibrational mode

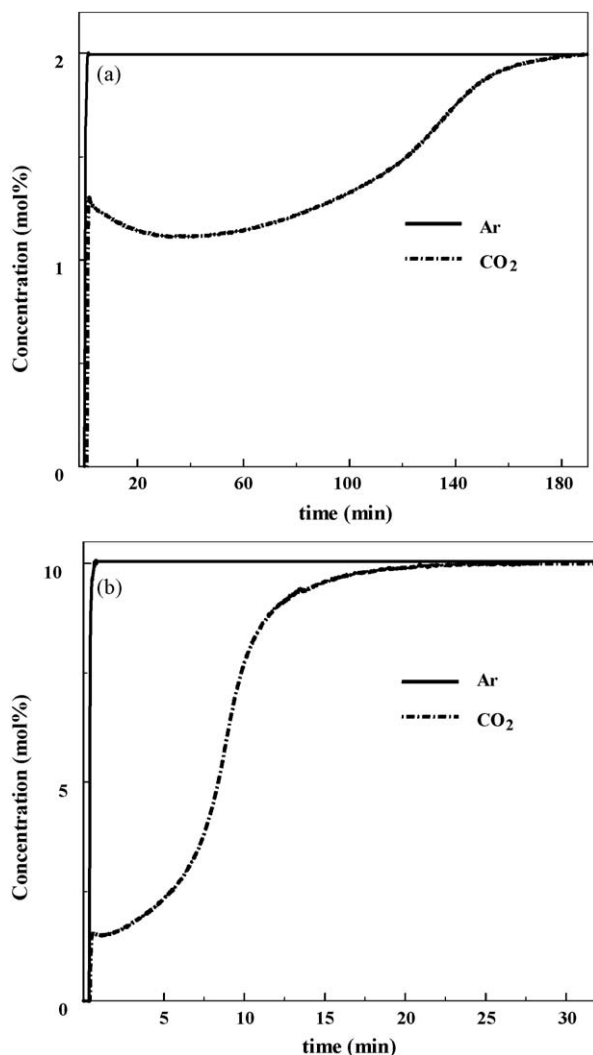**Fig. 11.** Transient response curves of $CO_2$ and Ar obtained at 650 °C according to the gas delivery sequence 20%$O_2$/He (800 °C, 2 h) → He (650 °C, 15 min) → x%$CO_2$/x%Ar/He (t), where (a) x = 2 and (b) x = 10 over the natural calcite material.

**Fig. 12.** (a) *In situ* DRIFTS spectra recorded in the 1800–1100 $cm^{-1}$ range after exposing the CaO surface of the natural calcite material on 2%$CO_2$/98%He gas mixture for 30 min at 25 °C and subsequently increasing the solid temperature under Ar flow up to 600 °C. DRIFTS spectra are shown for T = 100, 300 and 600 °C. (b) Integral band area corresponding to the three important carbonate species formed on the surface of natural calcite material according to (a).

of bridged carbonate [61,65–67], those at 1688 and 1640 $cm^{-1}$ to the OCO$_{as}$ vibrational mode of two different bicarbonate species ($HCO_3^{2-}$) (formed via interaction of $CO_2$ with surface –OH). The weaker IR bands centered at 1480 and 1442 $cm^{-1}$ are assigned to the OCO$_s$ vibrational modes of the same bicarbonates [61,66–69]. The IR bands centered at 1556, 1536 and 1393 $cm^{-1}$ correspond to the asymmetric vibrational mode of two different unidentate carbonate species and to the symmetric vibrational mode of unidentate carbonate ($CO_3^{2-}$), respectively, all associated with the basic surface $O^{2-}$ sites [66–70]. The broad weak IR band centered at 1233 $cm^{-1}$ is attributed to the COH bending vibrational mode of bicarbonate species [66,67].

The IR spectrum recorded at 100 °C shows that unidentate and bicarbonate species are the dominant adsorbed species on the CaO surface following $CO_2$ chemisorption at room temperature, in agreement with the literature [71]. It is important to note that no drastic change in the surface concentration of the various kinds of carbonate species formed was observed after increasing the desorption temperature from 25 to 100 °C in Ar flow (Fig. 12a) compared to the spectrum recorded at 25 °C under the $CO_2$/He treatment [40]. A decrease in the intensity of all IR bands was observed after heating the solid in Ar flow to 300 °C, where the most noticeable change was in the IR bands recorded at 1688 and 1640 $cm^{-1}$ (Fig. 12a). This is the result of the beginning of
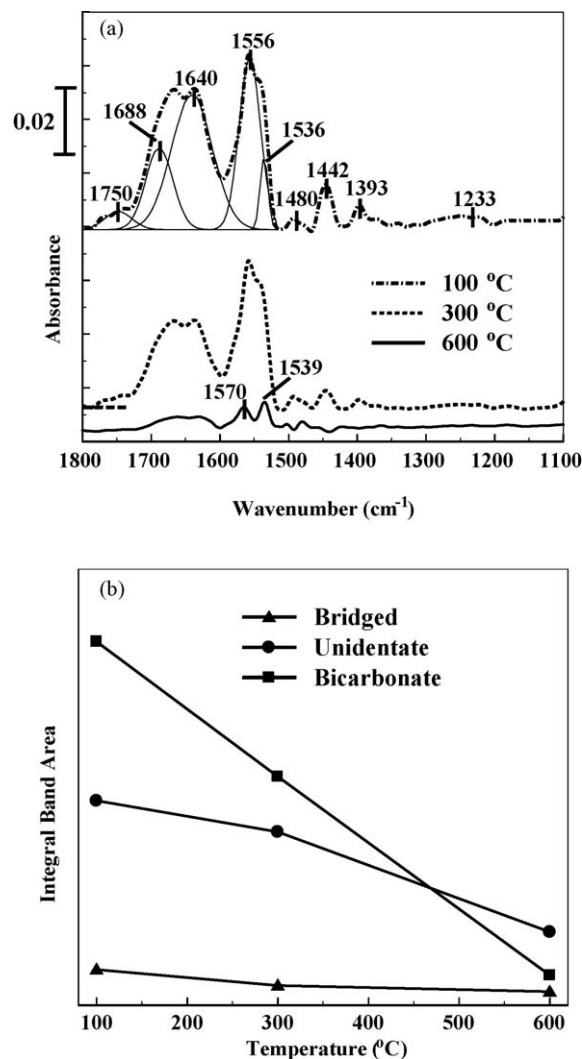
bicarbonate decomposition to release $CO_2$(g), where the former is known to exhibit a lower thermal stability than unidentate carbonates [61,66,67]. When the solid was heated to 600 °C in Ar flow the IR band centered at 1750 $cm^{-1}$ disappeared, all IR bands recorded in the 1500–1100 $cm^{-1}$ range were also absent, whereas the two overlapping bands corresponding to unidentate carbonates (1556 and 1536 $cm^{-1}$) can be resolved, indicating the beginning of their decomposition. The latter behavior may also indicate that a small amount of unidentate was converted to bidentate carbonate (1570 $cm^{-1}$), the latter being normally more stable than the unidentate carbonate structure [65,72] due to the lowering of the basic character of surface oxygen [65–67,73]. The TPD run shown in Fig. 12a (bottom graphs) illustrates that decomposition of the various carbonate structures formed after $CO_2$ chemisorption on CaO takes place mainly at high temperatures (T > 500 °C) in accordance with the TPD experimental response curves (Fig. 10).

Comparison of the integral band area of the most intense infrared carbonate bands obtained after deconvolution and curve fitting (e.g. upper spectrum in Fig. 12a) is presented in Fig. 12b. The integral band area of unidentate carbonates is considered as the

sum of the bands appeared in the 1600–1500 cm$^{-1}$ range, while that of bicarbonate as the sum of the bands appeared in the 1700–1600 cm$^{-1}$ range. It is seen that the surface coverage of bicarbonate species is higher than the surface coverage of unidentate and bridged carbonates, assuming similar extinction coefficients for the three $CO_2$ chemisorbed structures. It is noted that bicarbonate species appear as the weakest bonded carbonate-type structure on CaO. The latter is illustrated by the rate of change of its surface coverage with temperature when compared to the other two species (Fig. 12b). The fact that at 600 °C the surface coverage of unidentate is not zero but larger than that of bicarbonate, as opposed to the case at 100 °C, confirms the stability of the unidentate carbonate species at high temperatures.

### 3.7.2. Chemical structure and thermal stability of adsorbed surface carbonates formed under $CO_2/H_2O/H_2$ treatment

Fig. 13 compares the DRIFTS spectra recorded in the 1800–1100 cm$^{-1}$ range (K–M units) after a 30 min exposure of the pre-calcined surface of natural calcite material in different gas atmospheres at 600 °C: 2%$CO_2$/He, 2%$CO_2$/40%$H_2O$/He, and 2%$CO_2$/40%$H_2O$/30 or 50%$H_2$/He. More precisely, after 30 min of 2%$CO_2$/He gas treatment at 600 °C (Fig. 13a) a broad but small IR band centered at 1585 cm$^{-1}$ and a sharp larger IR band at 1542 cm$^{-1}$ are observed corresponding to bidentate and unidentate carbonates, respectively [68,69]. This is in harmony with the reported observation that bidentate carbonate species can also be formed on CaO when the temperature of adsorption is high [66,67,70,74]. It should be noted that the surface coverage of carbonates formed is larger compared to that obtained after $CO_2$ chemisorption at room temperature [40]. The latter is also in agreement with the fact that the $CO_2$ adsorption capacity of CaO increases with increasing temperature, as concluded from Figs. 10 and 11 and reported elsewhere [61].

$CO_2$ chemisorption in the presence of 40 vol% $H_2O$ (Fig. 13b) resulted in an increase and shift of the IR band corresponding to unidentate carbonates to slightly higher wavenumber (1558 cm$^{-1}$) compared to Fig. 13a (absence of water), having also a shoulder to the higher wavelength-side, suggesting the co-existence of bicarbonate (1620–1680 cm$^{-1}$), formate (OCO$_{as}$, 1600 cm$^{-1}$), and/or bidentate (1580 cm$^{-1}$) species [70]. This result is in agreement also with studies which reported that adsorption of pre-wetted $CO_2$ is more intensive than that of dry $CO_2$ [75]. In the case where

$CO_2$ adsorption was performed in the presence of 40 vol% $H_2O$ and 30 vol% $H_2$ (Fig. 13c), no significant change in the surface concentration of unidentate carbonate (1560 cm$^{-1}$) was observed, showing the strong bonding of this species on the catalyst surface, and, therefore, its higher thermal stability compared to the other formed carbonate structures (see also Fig. 12a). In addition, the comparison of Fig. 13b and c shows an increase in the intensity of the IR bands recorded at 1600 and 1335 cm$^{-1}$ and which are assigned to OCO$_{as}$ and OCO$_s$ of formate species, respectively, which can also be formed by $CO_2/H_2$ co-adsorption [70], and of the IR bands recorded in the 1620–1680 cm$^{-1}$ range corresponding to bicarbonate species. Therefore, the co-presence of 30 vol% $H_2$ and 2 vol% $CO_2$ in the adsorption mixture leads to an increase in the concentration of carbonate and formate species formed on the surface of CaO, lowering, therefore, the concentration of free surface active sites for phenol and water chemisorption.

After increasing the $H_2$ concentration to 50 vol% (Fig. 13d) in the $H_2/CO_2/H_2O$ gas adsorption mixture, the surface concentrations of bicarbonate and formate species were found to be largely reduced, while that of unidentate carbonate (1558 and 1537 cm$^{-1}$) remained practically the same. It is suggested that the large reduction in the concentration of formates formed in the presence of 50 vol% (Fig. 13d) compared to 30 vol% $H_2$ (Fig. 13c) in the $H_2/CO_2/H_2O$ gas adsorption mixture is related to the reduction in the concentration of –OH species formed on the CaO surface. The latter is confirmed by the IR spectral band of –OH groups formed upon water interaction with the CaO surface presented in Fig. 14.

According to the upper DRIFTS spectrum shown in Fig. 14, a broad IR band in the 3700–3400 cm$^{-1}$ region centered at 3500 cm$^{-1}$ is observed. In this specific region several kinds of –OH groups ($\nu$O–H stretching vibrational mode) which differ from each other in the degree of coordination by $Ca^{2+}$ in the first and by $O^{2-}$ in the second coordination spheres exist [76]. These –OH groups are formed via dissociative chemisorption of water on CaO. On the other hand, molecular adsorption of water (H-bonding mechanism) in which water molecule prefers to have an additional bond formed between its O atom and the next-neighbour surface $Ca^{2+}$ ion is also considered as energetically favorable [76]. Furthermore, multilayer adsorption of water molecules via H-bonding over metal oxides is possible, especially at high partial pressures of water [77]. In fact, Foster et al. [78] have studied by FTIR the multilayer adsorption of water on MgO(1 0 0) surface. A
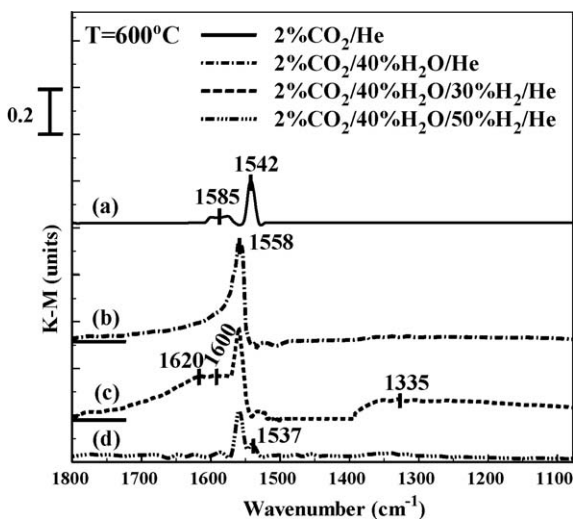


**Fig. 13.** *In situ* DRIFTS spectra recorded in the 1800–1100 cm$^{-1}$ range after 30-min exposure of the pre-calcined surface of the natural calcite material in (a) 2%$CO_2$/He, (b) 2%$CO_2$/40%$H_2O$/58%He, (c) 2%$CO_2$/40%$H_2O$/30%$H_2$/28%He, and (d) 2%$CO_2$/40%$H_2O$/50%$H_2$/8%He gas mixtures at 600 °C.
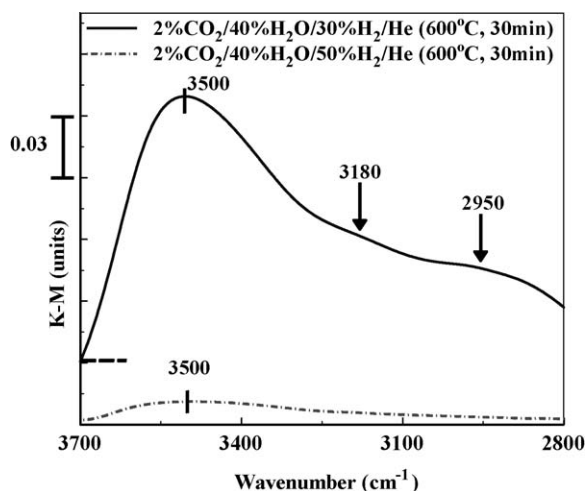


**Fig. 14.** *In situ* DRIFTS spectra recorded in the 3700–2800 cm$^{-1}$ range after 30 min exposure of the pre-calcined surface of the natural calcite material in 2%$CO_2$/40%$H_2O$/30%$H_2$/28%He and 2%$CO_2$/40%$H_2O$/50%$H_2$/8%He gas mixtures at 600 °C.

very similar IR band to that observed in the present work (Fig. 14), where the $\nu$O–H region appears in the 3700–2800 cm$^{-1}$ range was observed. Thus, extensive H-bonding between water molecules in multilayer adsorption mode causes large broadening of the $\nu$O–H region. It is noted that for gas-phase water, $\nu_s$O–H = 3657 cm$^{-1}$ and $\nu_{as}$O–H = 3756 cm$^{-1}$ [77], whereas strong absorption IR band due to $\nu$O–H in Ca(OH)$_2$ appears around 3600 cm$^{-1}$ [79]. The shoulder appeared at frequencies lower than 3000 cm$^{-1}$ and marked in Fig. 14 (upper spectrum) is partly due to the $\nu$C–H region of formate species as previously discussed.

Based on what mentioned in the previous paragraph, the effect of the presence of a large concentration of H$_2$ (e.g. 50 vol%) on the interaction of water molecules with the surface of CaO in a CO$_2$/H$_2$O/He gas adsorption mixture seems to be the hindrance in the formation of H-bonding between water molecules themselves and with the CaO surface, thus reducing significantly the formation of –OH groups needed for phenol steam reforming (see Figs. 4 and 5). In fact, comparing the catalytic results of Figs. 4a and 5 it is seen that the H$_2$ inhibiting effect becomes less important when the water concentration in the feed is increased (40 vol%, Fig. 4a vs. 50 vol%, Fig. 5). It is out of the scope of the present work to offer detailed mechanistic view of this hydrogen inhibiting effect on the chemisorption of water on the CaO surface.

### 3.8. Chemisorption aspects of $C_6H_5OH$, $CO_2$, $H_2O$ and $H_2$ on the surface of CaO

Scheme 1 provides the adsorption mode of phenol expected during steam reforming on a CaO surface (Scheme 1a), the structure of three important surface carbonate species formed due to the interaction of CO$_2$ with the CaO surface (Scheme 1b) according to the present results, and the sites and products of water (Scheme 1c) and hydrogen (Scheme 1d) more favorable dissociative adsorption routes on the CaO surface.

Scheme 1a illustrates a two-site adsorption mode associated with the interaction of the benzene ring, which is lying parallel to
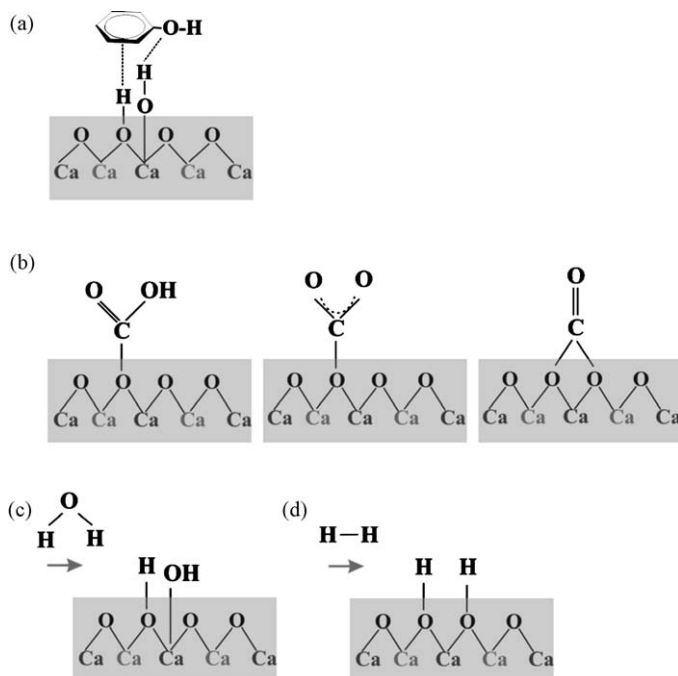
the surface with a surface hydroxyl group, and with the interaction of the substitute group (–OH) with a neighbouring surface hydroxyl group. The latter species is reported [80] to be formed on metal oxide surfaces through water dissociation during steam reforming of phenol. The dual-site mechanism of phenol adsorption has also been proposed in the literature [81–83] for other tar species, like chlorobenzene and phenatrene related to the surfaces of ZnO and CaO, respectively. As a result of this adsorption mode, the opening of the benzene ring and the formation of H$_2$, CO, CO$_2$ and other adsorbed $C_xH_y$ species occur.

According to Scheme 1b, CO$_2$ reacts predominantly with O$^{2-}$ and OH$^-$ sites of the CaO surface producing mainly unidentate and bicarbonate species, and at a lower extent bridging carbonate species as concluded from the in situ CO$_2$-DRIFTS experiments (Figs. 12 and 13). The unidentate carbonate was found to be strongly bound on the catalyst surface and it is readily formed compared to the other kinds of carbonates, even at high temperatures and using CO$_2$/H$_2$O/H$_2$ gas mixtures. The surface concentration of the carbonate species changes with temperature and gas composition (CO$_2$/H$_2$O/H$_2$).

Water is dissociatively chemisorbed on the calcium oxide surface according to Scheme 1c producing –OH groups on top of Ca$^{2+}$ ions and a lower layer hydroxyls associated to lattice oxygen anions [53,54,80]. Heterolytic splitting of molecular H$_2$ onto a Ca$^{2+}$–O$^2$ ion pair [53,54] leads to the formation of –OH groups associated only to lattice oxygen anions as illustrated in Scheme 1d. Therefore, water and hydrogen compete for chemisorption for the same surface O$^{n-}$ active sites. However, the extent of competitive adsorption of H$_2$ and H$_2$O depends on the partial pressures of the two adsorbates, the adsorption temperature, and the heat of adsorption. Furthermore, the H-bonding effects discussed in the last paragraph of Section 3.7.2 should also be considered.

## 4. Conclusions

The following conclusions can be derived from the results of the present work:

(a) The catalytic activity of natural calcite material calcined at 850 °C in 20%O$_2$/He for 2 h towards phenol steam reforming is not due to the inherent metal impurities (<0.4 at%) present.

(b) The increase of reaction temperature in the 650–800 °C range increases phenol steam reforming activity and selectivity towards H$_2$, whereas phenol conversion and hydrogen selectivity both increase with decreasing GHSV in the 40,000–80,000 h$^{-1}$ range.

(c) An increase of water feed concentration in the 40–50 vol% range increases the hydrogen reaction yield in the 650–800 °C range. The effect of H$_2$ concentration (10–50 vol%) in the feed stream (0.6 vol%C$_6$H$_5$OH/30 or 40 vol% H$_2$O/He) on phenol steam reforming activity appears to be strongly negative, while this effect becomes smaller for a water feed concentration of 50 vol%. A similar negative effect was evident with the carbon dioxide concentration in the feed stream.

(d) The initial activity of the pre-calcined natural calcite material (CaO) dropped during the first six consecutive oxidation (850 °C)/reaction (680 °C) cycles due to carbon accumulation on the catalyst surface which was found to increase with reaction time from 5 to 20 min. No practical drop in activity was obtained after the sixth oxidation/reaction cycle.

(e) The rate of phenol steam reforming at steady-state reaction conditions was found to be inversely proportional to the partial pressure of CO$_2$ used in the feed stream. The characteristic features of the transient evolution of H$_2$ product suggests that adsorbed CO$_2$ formed on the CaO surface influences the kinetics of phenol steam reforming.



**Scheme 1.** (a) The dual-site adsorption mode of phenol during steam reforming reaction, (b) the structure of surface carbonate species formed upon CO$_2$ adsorption on pre-calcined natural calcite material (CaO), (c) the decomposition of water, and (d) the decomposition of hydrogen on CaO surface.

(f) *In situ* DRIFTS-$CO_2$ chemisorption studies ($CO_2$/He gas mixtures) demonstrated the existence of unidentate, bicarbonate and bridged carbonates as the three main carbonate structures of chemisorbed carbon dioxide, where unidentate appears to be the main carbonate-like structure even in the high temperature of 600 °C.

(g) A substantial decrease in the surface concentration of bicarbonate and –OH groups was observed when adsorption of $CO_2$ took place from a gas mixture containing 40 vol% $H_2O$ and $H_2$ in the 0–50 vol% range (feed stream 2%$CO_2$/40%$H_2O$/$x$%$H_2$/He). The latter result establishes the strong inhibiting effect of $H_2$ on the reaction rate observed when hydrogen is co-fed in the phenol/water reaction gas mixture.

(h) Water and hydrogen molecular species compete for the same sites for dissociation on CaO at 600 °C, the rate of each step being dependent on the partial pressure of $H_2O$ and $H_2$, giving rise to the catalytic effects concluded in (c).

(i) The results of the present work illustrate that natural calcites (cheap, non-toxic) can be considered as potential materials in industrial biomass and waste-biomass gasification plants for the purification from tars of the $H_2$-rich gas produced (via steam reforming reaction). The surface morphology of the CaO derived from the calcination of calcite plays an important role on its reforming activity [40], as well as the concentration of $H_2$ and $CO_2$ present in the purifying gas (0–30 vol%).

## Acknowledgement

## References

[1] H. Boerrigted, R. Rauchin, Syngas Production and Utilization, Biomass Technology Group (BTG), Netherlands, 2005 (Chapter 10).
[2] K. Möllersten, J. Yan, J.R. Moreira, Biomass Bioenergy 25 (2003) 273.
[3] T. Marquard-Möllenstedt, U. Zuberbuchler, M. Specht, in: Proceedings of 16th European Biomass Conference and Exhibition from Research to Industry and Markets, Valencio, 2–6 June, (2008), pp. 684–689.
[4] T. Marquard-Möllenstedt, P. Sichler, M. Specht, M. Michel, R. Berger, K.R.G. Heim, H. Höftberger, R. Rauch, H. Hofbauer, in: Proceedings of 2nd World Conference on Biomass for Energy Climate, Industry, Climate Protection, Rome, 10–14 May, (2004), pp. 758–762.
[5] L. Devi, K.J. Ptasinski, F.J.J.G. Janssen, Biomass Bioenergy 24 (2003) 125.
[6] C. Courson, L. Udron, D. Świerczyński, C. Petit, A. Kiennemann, Catal. Today 76 (2002) 75.
[7] D. Sutton, B. Kelleher, J.R.H. Ross, Fuel Proc. Tech. 73 (2001) 155.
[8] J.N. Armor, Appl. Catal. A: Gen. 176 (1999) 159.
[9] M.A. Peña, J.P. Gómez, J.L.G. Fierro, Appl. Catal. A: Gen. 144 (1996) 7.
[10] D. Dayton, A Review of the Literature on the Catalytic Biomass Tar Destruction, NREL/TP-510-32815, National Renewable Energy Laboratory, 2002.
[11] L. Garcia, M.L. Salvador, J. Arauzo, R. Bilbao, Energy Fuels 13 (1999) 851.
[12] S. Rapagnà, N. Jand, P.U. Foscolo, Int. J. Hydrogen Energy 23 (1998) 551.
[13] R. Zhang, R.C. Brown, A. Suby, K. Cummer, Energy Convers. Manage. 45 (2004) 995.
[14] J. Corella, A. Orío, J.-M. Toledo, Energy Fuels 13 (1999) 702.
[15] L. Garcia, M.L. Salvador, J. Arauzo, R. Bilbao, Fuel Proc. Tech. 69 (2001) 157.
[16] T.A. Milne, N. Abatzoglou, R.J. Evans, Biomass Gasifier Tars: Their Nature, Formation and Conversion, NREL/TP-570-25357, National Renewable Energy Laboratory, USA, 1989.
[17] European Project, 6th FP, No. 5183309 (SES6), Biomass Fluidized Bed Gasification with In-Situ Hot Gas Cleaning, 2006.
[18] C. Brage, Q. Yu, K. Sjöström, Fuel 75 (2) (1996) 213.
[19] D. Wang, S. Czernik, D. Montané, M. Mann, E. Chornet, Ind. Eng. Chem. Res. 36 (1997) 1507.
[20] J. Corella, A. Orío, M.-P. Aznar, Ind. Eng. Chem. Res. 37 (1998) 4617.
[21] S. Rapagná, H. Provendier, C. Petit, A. Kiennemann, P.U. Foscolo, Biomass Bioenergy 22 (2002) 377.
[22] R. Coll, J. Salvadó, X. Farriol, D. Montané, Fuel Proc. Technol. 74 (2001) 19.
[23] I. Alstrup, M.T. Tavares, J. Catal. 135 (1992) 147.
[24] D.L. Trimm, Catal. Today 49 (1999) 3.
[25] G. Hu, S. Xu, S. Li, C. Xiao, S. Liu, Fuel Proc. Tech. 87 (2006) 375.
[26] J. Delgado, M.-P. Aznar, J. Corella, Ind. Eng. Chem. Res. 35 (1996) 3637.
[27] J. Delgado, M.-P. Aznar, J. Corella, Ind. Eng. Chem. Res. 36 (1997) 1535.
[28] D. Swierczynski, S. Libs, C. Courson, A. Kiennemann, Appl. Catal. B: Environ. 74 (2007) 211.
[29] J.N. Kuhn, Z. Zhao, L.G. Felix, R.B. Slimane, C.W. Choi, U.S. Ozkan, Appl. Catal. B: Environ. 81 (2008) 14.
[30] V. Vassilatos, G. Taralas, K. Sjöström, E. Björnborm, Can. J. Chem. Eng. 70 (1992) 1008.
[31] P. Pérez, P.-M. Aznar, M.A. Caballero, J. Gill, J.A. Martin, J. Corella, Energy Fuels 11 (1997) 1194.
[32] I. Narváez, A. Orío, M.-P. Aznar, J. Corella, Ind. Eng. Chem. Res. 35 (1996) 2110.
[33] J. Corella, J.-M. Toledo, R. Padilla, Energy Fuels 18 (2004) 713.
[34] G. Taralas, V. Vassilatos, K. Sjöström, J. Delgado, Can. J. Chem. Eng. 69 (6) (1991) 1413.
[35] X. Garcia, N.A. Alarcon, A.L. Gordon, Fuel Proc. Tech. 58 (1999) 83.
[36] P.A. Simell, J.K. Leppälahti, J.B.S. Bredenberg, Fuel 71 (2) (1992) 211.
[37] M.R. Mahishi, D.Y. Goswami, Int. J. Hydrogen Energy 32 (2007) 2803.
[38] B. Balasubramanian, A.L. Ortiz, S. Kaytakoglu, D.P. Harrison, Chem. Eng. Sci. 54 (1999) 3543.
[39] C. Pfeifer, B. Puchner, H. Hofbauer, Inter. J. Chem. Rec. Eng. 5 (2007) A9.
[40] D.A. Constantinou, A.M. Efstathiou, Catal. Today, in press (available on line).
[41] A.L. Patterson, Phys. Rev. 56 (1939) 978.
[42] C.N. Costa, T. Anastasiadou, A.M. Efstathiou, J. Catal. 194 (2000) 250.
[43] K. Polychronopoulou, C.N. Costa, A.M. Efstathiou, Appl. Catal. A: Gen. 272 (2004) 37.
[44] K. Polychronopoulou, J.L.G. Fierro, A.M. Efstathiou, J. Catal. 228 (2004) 417.
[45] K. Polychronopoulou, A. Bakandritsos, V. Tzitzios, J.L.G. Fierro, A.M. Efstathiou, J. Catal. 241 (2006) 132.
[46] A.M. Efstathiou, Ph.D. Thesis, University of Connecticut, USA, 1989.
[47] B.C. Smith, Fundamentals of Fourier Transform Infrared Spectroscopy, CRC Press, 1996.
[48] K. Chrissafis, C. Dagounaki, K.M. Paraskevopoulos, Thermochim. Acta 428 (2005) 193.
[49] K. Kuramoto, S. Fujimoto, A. Morita, S. Shibano, Y. Suzuki, H. Hatano, L. Shi-Ying, M. Harada, T. Takarada, Ind. Eng. Chem. Res. 42 (2003) 975.
[50] M.P. Seah, D. Briggs (Eds.), Practical Surface Analysis, John Wiley Sons, Chichester, 1990.
[51] H. Aldén, E. Björkman, M. Carlsson, A. Waldheim, in: Proceedings of Conference on Advances in Thermochemical Biomass Conversion, Blackie Academic & Professional, London, 1994, p. 216.
[52] G. Taralas, Ind. Eng. Chem. Res. 35 (1996) 2121.
[53] H. Hattori, Chem. Rev. 95 (1995) 537.
[54] H. Kobayashi, M. Yamaguchi, T. Ito, J. Phys. Chem. 94 (1990) 7206.
[55] P.A. Simell, E.K. Hirvensalo, V. Smolander, A.O.I. Krause, Ind. Eng. Chem. Res. 38 (1999) 1250.
[56] P.A. Simell, J.O. Hepola, A.O.I. Krause, Fuel 76 (12) (1997) 1117.
[57] A. Jess, Fuel 75 (12) (1996) 1441.
[58] X.A. Garcia, K.J. Hüttinger, Fuel 68 (1989) 1300.
[59] S. Adhikari, S. Fernando, A. Haryanto, Catal. Today 129 (2007) 355.
[60] X. Garcia, K.J. Hüttinger, Erdöl Kohle Endgas Petrochem. 43 (1990) 273.
[61] Y. Xu, L. Yu, C. Cai, J. Huang, X. Guo, Catal. Lett. 35 (1995) 215.
[62] P.A. Simell, J.K. Leppälahti, E.A. Kurkela, Fuel 74 (6) (1995) 945.
[63] M. Specht, A. Bandi, F. Baumgart, T. Moellenstedt, O. Textor, T. Weimer, in: Z.Q. Mao, T.N. Veziroglou (Eds.), Hydrogen Energy Process XIII, 2000, p. 1203.
[64] G. Zhang, H. Hattori, K. Tanabe, Appl. Catal. 36 (1988) 189.
[65] N. Alarcón, X. Garcia, M. Centeno, P. Ruiz, A. Gordon, Surf. Interf. Anal. 31 (2001) 1031.
[66] R. Philipp, K. Fujimoto, J. Phys. Chem. 96 (1992) 9035.
[67] R. Philipp, K. Omata, A. Aoki, K. Fujimoto, J. Catal. 134 (1992) 422.
[68] M.I. Zaki, H. Knözinger, B. Tesche, G.A.H. Mekhemer, J. Colloid Interf. Sci. 303 (2006) 9.
[69] M.I. Zaki, H. Knözinger, B. Tesche, G.A.H. Mekhemer, H.-J. Bongard, Langmuir 24 (2008) 6745.
[70] G. Busca, V. Lorenzelli, Mater. Chem. 7 (1982) 89.
[71] P. Käβner, M. Baerns, Appl. Catal. A: Gen. 139 (1996) 107.
[72] J.C. Lavalley, Catal. Today 27 (1996) 377.
[73] A.A. Davydov, Catal. Today 24 (1995) 225.
[74] Y. Fukuda, K. Tanabe, Bull Chem. Soc. Jpn. 46 (1973) 1616.
[75] A.A. Medvinskii, G.G. Saveliev, N.F. Stas', O.V. Tyunina, V.V. Nakhalov, I.A. Kononova, P.D. Khalfma, React. Kinet. Catal. Lett. 6 (2) (1977) 139.
[76] N.U. Zhanpeisov, H. Nakatsuji, M. Hada, J. Mol. Catal. A: Chem. 112 (1996) 63, and references therein.
[77] P.A. Thiel, T.E. Madey, Surf. Sci. Rep. 7 (1987) 211, and references therein.
[78] M. Foster, M. Furse, D. Passno, Surf. Sci. 502–503 (2002) 102.
[79] P. Lagarde, M.A.H. Nerenberg, Y. Farge, Phys. Rev. B 8 (4) (1973) 1731.
[80] M.J. Low, N. Takezawa, A.J. Goodsel, J. Colloid Interf. Sci 37 (2) (1971) 422.
[81] J. Corella, M.A. Caballero, M.-P. Aznar, C. Brage, Ind. Eng. Chem. Res. 42 (2003) 3001.
[82] T. Morimoto, Y. Suda, M. Nagaot, J. Phys. Chem. 89 (1985) 4881.
[83] W. Pohle, J. Chem. Soc. Faraday Trans. 78 (1982) 2101.